PAPER • OPEN ACCESS

Effect of toroidal plasma currents on the Wendelstein 7-X Scrape-Off Layer

View the article online for updates and enhancements.

IOP ebooks™

Bringing you innovative digital publishing with leading voices to create your essential collection of books in STEM research.

Start exploring the collection - download the first chapter of every title for free.

Effect of toroidal plasma currents on the Wendelstein 7-X Scrape-Off Layer

Carsten Killer[1] , **Yu Gao**[2] , **Valeria Perseo**[1] , **Lukas Rudischhauser**[1] ,
Kenneth Hammond[1] , **Birger Buttenschön**[1] , **Tullio Barbui**[3],
Boyd D Blackwell[4], **Kai-Jakob Brunner**[1], **Philipp Drews**[2] ,
Michael Endler[1] , **Joachim Geiger**[1] , **Olaf Grulke**[1,5],
Marcin Jakubowski[1] , **Sören Klose**[1], **Jens Knauer**[1] , **Alexander Knieps**[2],
Ralf König[1], **Yongliang Li**[2], **Ulrich Neuner**[1], **Holger Niemann**[1] ,
Matthias Otte[1] , **Jonathan Schilling**[1], **Aleix Puig Sitjes**[1],
Kian Rahbarnia[1] , **Torsten Stange**[1] **and W7-X Team**[1,6]

[1] Max-Planck-Institut für Plasmaphysik, Greifswald, Germany
[2] Forschungszentrum Jülich, IEK-4 Plasmaphysik, Jülich, Germany
[3] Princeton Plasma Physics Laboratory, Princeton, NJ 08540, United States of America
[4] Australian National University, Canberra ACT 2600, Australia
[5] Department of Physics, Technical University of Denmark, Lyngby, Denmark

E-mail: carsten.killer@ipp.mpg.de

CrossMark

Abstract

The role of toroidal plasma currents for the island divertor scrape-off layer in the stellarator Wendelstein 7-X is investigated using reciprocating electric probes. Experiments show that small amounts (of a few kA) of plasma current are sufficient to significantly affect the scrape-off layer plasma conditions, whereas higher plasma currents above 10kA result in more drastic changes. This behavior is linked to the effect of the plasma current on the rotational transform profile, which can result in significant shifts of the edge magnetic islands. These shifts affect the interaction of the islands with the divertor and can eventually result in a transition from a diverted to a limited plasma configuration. The probe observations are complemented by further edge diagnostics including plasma flow measurements, divertor Langmuir probes, divertor thermography and impurity spectroscopy.

Keywords: stellarator, Scrape-Off Layer, reciprocating probe, island divertor

(Some figures may appear in colour only in the online journal)

1. Introduction

In stellarators, the confining magnetic field is entirely created by the external coils. Net plasma currents are usually avoided as they can act as a source of free energy, potentially affecting

---

[6] see T. Klinger, *Nucl. Fusion* **59** (2019) 112004.

plasma stability. Especially in low shear stellarators employing island divertors [1], the minimization of toroidal plasma currents is even more important. There, the resonant magnetic islands at the plasma edge which determine the heat and particle exhaust to the divertors are particularly sensitive to even slight changes in the rotational transform (ι) profile. Therefore, minimization of the bootstrap current was one of the optimization criteria for the design of the optimized stellarator Wendelstein 7-X (W7-X) [2].

Depending on the particular magnetic configuration of W7-X, the equilibrium bootstrap current ranges between vanishing values $<1\,$kA and substantial values of some $10\,$kA
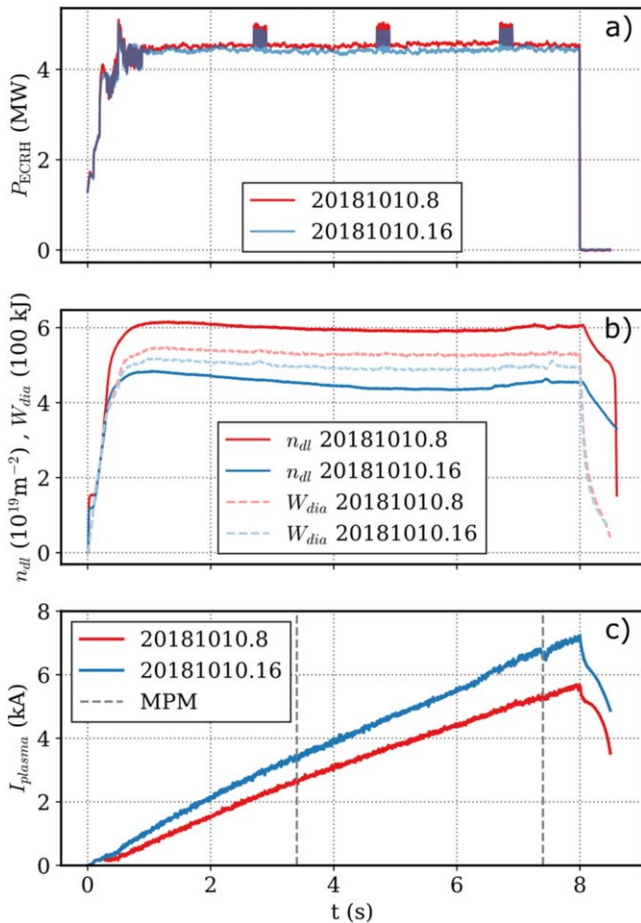
Figure 1. Time traces of (a) ECRH power, (b) line integrated density (solid) and diamagnetic energy (dashed), (c) toroidal plasma current for two programs in the standard configuration. The time instances of the MPM measurements are indicated by the vertical lines in (c). The features around 3 s, 5 s and 7 s in (a) are quick modulations of the heating power for diagnostic purposes (not relevant here) and do not affect the SOL plasma properties.

[3], which can already significantly affect the edge magnetic topology and result in large shifts of the strike lines on the divertors [4, 5]. While in most cases the island divertor is designed such that both the vacuum case (no toroidal plasma current) and the equilibrium case (fully evolved toroidal plasma current) are suited operation scenarios, the transient phases of the bootstrap current evolution can feature critical heat load to in-vessel components. This transient phase is defined by the decay of shielding currents (which initially shield the bootstrap current) and takes place on the L/R time scale which is some 10 s for W7-X [4, 6]. Measurements of the bootstrap current with a continuous Rogowski coil agree qualitatively well and quantitatively reasonably with theoretical predictions [7, 8]. Mitigation strategies explored so far include the use of electron cyclotron current drive (ECCD) to either compensate the bootstrap current or accelerate the transient phase towards an equilibrium current [5, 9, 10], or implementing sophisticated plasma heating and fuelling control schemes [11]. Another approach is the installation of additional divertor components (so-called scraper elements)

which are supposed to protect sensitive components during the transient current evolution phase [12, 13].

First experiments during the initial divertor operation phase of W7-X in 2017/2018 have shown that the strike line dynamics caused by the toroidal current evolution behave largely as expected [14]. However, some new open questions emerged from these experiments, e.g. regarding the role of particle drifts and error fields in the intricate interplay of the island divertor plasma conditions and magnetic topology. Therefore, investigating the conditions and processes in the (upstream) scrape-off layer (SOL) is fundamental for understanding and eventually controlling the heat and particle fluxes to the divertor.

Here, we report on experiments on the role of toroidal plasma currents for the SOL plasma conditions. Section 2 is devoted to the influence of the evolution of the intrinsic bootstrap current on the SOL, covering the experimentally available range of up to 7 kA. A combination of divertor diagnostics (target probes, thermography) and SOL/edge diagnostics (reciprocating probes, Coherence Imaging Spectroscopy) is employed to gain a comprehensive picture of plasma conditions in the three-dimensional (3D) SOL of W7-X. In section 3, the effect of larger toroidal currents obtained with ECCD is explored in a more brief manner, due to limited data availability.

2. Intrinsic plasma currents

While the magnetic coil set of W7-X allows to adjust configurations with respect to the rotational transform or the mirror ratio in a wide range [3], we focus here on the so-called *standard configuration* which was the most frequently used one in the recent operation phases (2017/2018). The standard configuration features a chain of five independent, resonant magnetic islands at the edge with the edge rotational transform crossing the rational value $\iota_{edge} \approx 5/5$. The islands are intersected by the modular divertor according to the island divertor concept [15]. In the first two operation phases with uncooled divertor modules (OP1.2a/b), the island divertor concept turned out to work as designed, with a favourable distribution of heat fluxes and first detachment results [16]. A notable characteristic of the standard configuration is the evolution of significant bootstrap currents, which are predicted be on the order of 10 kA, depending on the plasma conditions [3]. For moderate plasma currents up to $I_p = 5$ kA, the strike lines on the divertors were observed to move in a manner that is consistent with field line diffusion calculations which include both the vacuum magnetic field and the contribution from the plasma current [14].

Reciprocating probe measurements close to the outer mid-plane [17] have shown that the radial profiles of electron temperature and plasma density are strongly affected by the presence of magnetic islands. In the standard configuration, where the probe crosses a magnetic island, the SOL is found to be a few cm wide, with quite flat plasma pressure profiles across the magnetic island [18, 19]. The tendency of magnetic islands flattening temperature profiles is well known from

both stellarators and tokamaks [20–22]. Also, first hints on the role of even small plasma current changes (≈ 1 kA) for the SOL plasma profiles have been observed experimentally [18, 19]. In contrast, in so-called *limiter-like* configurations, where due to the absence of edge magnetic islands the last closed flux surface is defined by the intersection of the main plasma with the divertor, the SOL is only a few mm wide and does not show any significant response to plasma currents in the experimentally covered range up to 7 kA [18].

To study the role of the toroidal current evolution on the island divertor SOL, we here focus on two plasma programs presented in figure 1. The nomenclature of W7-X discharges (called *programs*) in the labels of this and following figures is based on the date of the experiment (year-month-day) and the number of the program on that day. In both programs, the electron cyclotron resonance heating (ECRH) and the hydrogen plasma density and diamagnetic energy in the plasma were kept constant. Different gas puffing levels during plasma ignition resulted in different line integrated densities. The toroidal plasma current is dominated by the bootstrap current as there was no ECCD in these experiments. The plasma current is measured by a continuous Rogowski coil [23] and is in these experiments still far from saturation since $L/R \approx 15$ s. Besides the evolution of the plasma current, the plasmas are essentially stationary up to their scheduled termination after 8 s.

2.1. Reciprocating probe measurements

The multi-purpose manipulator (MPM) [17] equipped with a multi-functional probe head (IPP-FLUC1 [18]) probed each plasma with a fast plunge into the edge island twice, at the time instances indicated by the dashed vertical lines in figure 1(c). The resulting probe data is shown in figure 2 as a function of the major radius along the probe path. The electron temperature and density profiles have been obtained using a triple Langmuir probe. For the density calculation, a simple isothermal pure hydrogen plasma (charge $Z = 1$, ion mass $m_i = m_p$, $T_e = T_i$, adiabatic coefficient $\gamma = 1$) has been assumed. Since reliable profiles of these values are not yet available for W7-X, we refrain from making any estimations and note that with the simple assumptions made here the plasma density is probably over-estimated by 15% to 30%.

At the first plunge (at T1 = 3.4 s with plasma currents around 3 kA), represented by lighter colors, the electron temperature (T_e) profiles align well in both programs, with a local maximum close to $R = 6.08$ m that is characteristic for the standard configuration and is attributed to the magnetic island topology [18]. The density profiles in figure 2(b) are at T1 relatively shallow with their magnitudes representing the different line integrated density levels of the two plasma programs, again similar to earlier investigations [18].

At the second measurement at elevated plasma currents at T2, T_e and n are found to be increased in both programs with respect to the situation at T1. However, a much stronger increase of T_e and n is observed in program 20 181 010.16 (with higher plasma current), such that now higher T_e and n are seen in the program with lower line integrated density. At
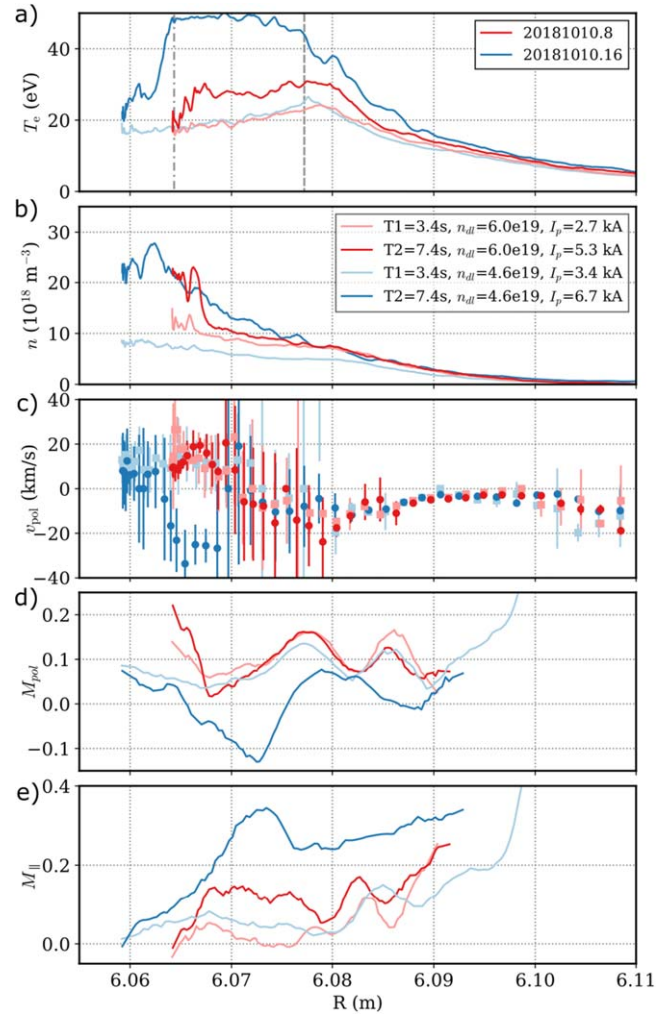

Figure 2. Radial profiles along the probe path of (a) electron temperature T_e, (b) plasma density n, (c) poloidal phase velocity, (d) poloidal Mach number, (e) parallel Mach number for the probe plunges indicated by the dashed lines in figure 1. The vertical dashed and dashed-dotted lines in the top panel correspond to the similarly styled lines in figure 3.

the same time, the core plasma profiles remain unaffected by this evolution (so that the almost constant n_{dl} and W_{dia} in figure 1 are a good proxy for describing the core plasma). This indicates that the changes seen by the reciprocating probe are localized to the SOL and in particular to the position of the probe. A more general diagnostic approach to the SOL plasma will be attempted in section 2.3. Although a qualitatively similar observation of increased T_e and n correlating with increasing plasma current is observed by the thermal helium beam spectroscopy [24], no direct comparison of both diagnostics is attempted here due to the complex 3D mapping, but will be discussed in a future article. The significant heat flux to the probe head at T2 in program 20 181 010.16 at $T_e \approx 50$ eV and $n \approx 2 \cdot 10^{19}$ m^{-3} resulted in a considerable release of impurities (mostly boron and nitrogen from the probe head body), perturbing the plasma for some 100 ms, as seen in the time traces of density, diamagnetic energy and plasma current in figure 1. Since the disturbance of the plasma occurred during the retracting, second part of the plunge, we

only consider the first part when the probe moves towards the plasma in all data shown in figure 2.

Further properties obtained from the multi-functional probe head [18] include the poloidal phase velocity v_{pol} of fluctuations propagating along the poloidal probe array as well as parallel and poloidal Mach numbers as presented in figures 2(c)–(e). The v_{pol} profiles can be taken as a measure for the radial electric field assuming that the poloidal dynamics are $E_r \times B$ driven [25]. In the outer parts of the profiles in figure 2(c), negative phase velocities are observed (here being defined as upwards directed in the lab frame) which correspond to positive (outwards directed) electric fields, as expected in the SOL. The sign of v_{pol} then flips around $R = 6.07$ m as the probe crosses the edge island, indicating an inwards directed field inside the island [18]. An exception is observed in the measurement at the highest plasma current, where a significant excursion to strongly negative v_{pol} (and therefore highly positive E_r) is observed between $R = 6.065$ m and $R = 6.07$ m. This observation is mirrored by the negative excursion of the poloidal Mach number data of the same program in figure 2(d) around $R = 6.07$ m, since the poloidal Mach number is defined such that negative values describe an upwards flow which is consistent with positive E_r via $E_r \times B$ flow. The parallel Mach number profiles in figure 2(e) in general decrease as the probe moves from the outer SOL closer towards the LCFS as expected from EMC3-Eirene simulations [26]. In both programs, the parallel Mach number is found to increase at T2 compared to T1, again with a stronger increase in program 16 featuring a higher plasma current. Apart from these observations, the general modulated shape of both the poloidal and parallel Mach number profiles are not well understood yet and require further investigations such as modeling of the 3D SOL with EMC3-Eirene in realistic plasma conditions and magnetic field structures.

2.2. Modeling plasma current via field line tracing

The importance of a detailed look into the edge magnetic field topology is corroborated by figure 3, which displays the connection length along the magnetic field in the vicinity of the probe path in the R-z plane for different toroidal plasma currents in the magnetic standard configuration. The connection length is defined as the distance along a field line between a chosen start point (in this case the start points are located in a 2D plane around the probe) and the location where the respective field line is intersected by a physical object, i.e. a divertor or wall element. Regions of closed field lines (i.e. infinite connection lengths) are shown in light grey. For these calculations, the plasma current has been prescribed to the magnetic axis, neglecting the spatial distribution of the plasma current. This simplification is justified by Ampère's Law, since we are here only interested in the effects of currents in the confined plasma on the magnetic field in the SOL, i.e. outside the confined plasma. Nevertheless, second order effects caused by the current profile, such as changes of the iota profile's shear, might play a (smaller) role on the SOL connection length distribution. Covering these finer details by
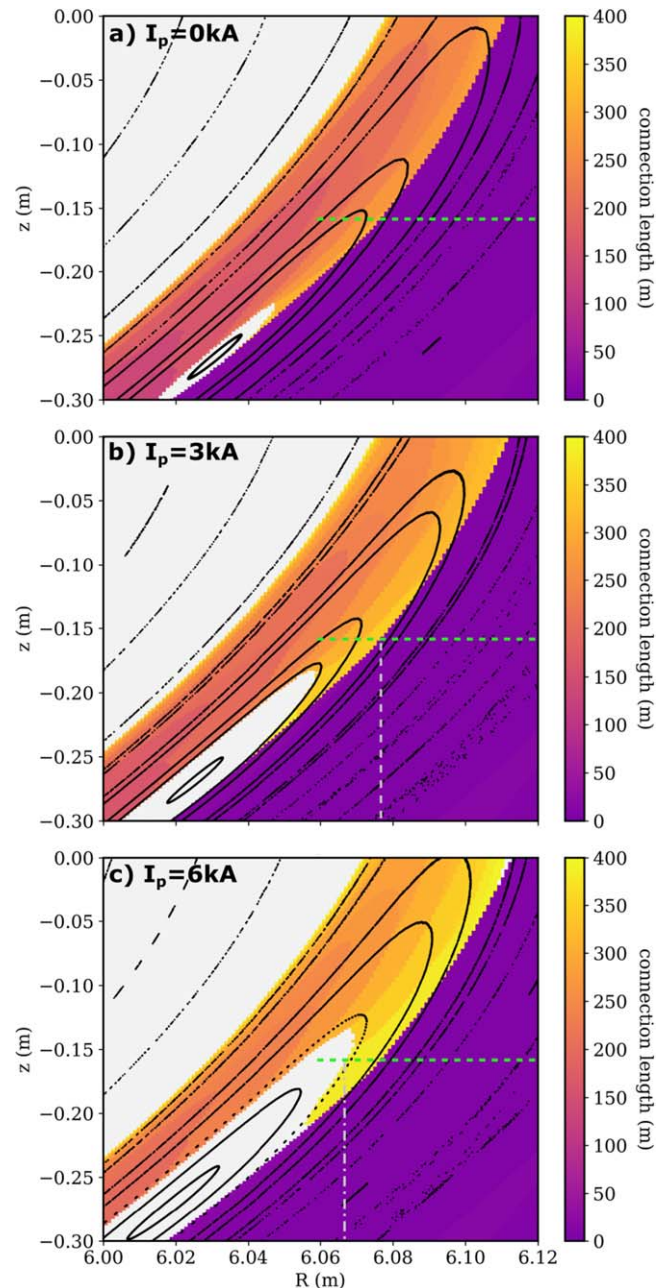

Figure 3. Poincaré plot (black dots) and connection lengths (color coded) in the R-z plane around the probe path in the W7-X standard configuration for different toroidal plasma currents, (a) 0 kA, (b) 3 kA, (c) 6 kA. Light grey areas indicate closed field lines, i.e. infinite connection lengths. The probe path is indicated by the dashed green lines. While these results are generic, (b) resembles the situation at the T1 measurements in figure 2 and (c) resembles the T2 measurement of 20 181 010.16. The grey vertical lines in (b) and (c) correspond to the similarly styled lines in figure 2(a).

modeling is, however, beyond the scope of this paper as the current profiles in W7-X show in general a wide variability [3, 4], and the impact of current distribution on the iota profile competes with other second order effects such as finite plasma pressure.

Comparing the three different situations displayed in figure 3, the edge magnetic island (and the last closed flux surface) is found to move slightly inwards at higher plasma

currents, as seen from the Poincaré plots represented by the black dots (at the probe position the shift is about 2 mm per kA plasma current). This inwards shift of the island is expected as positive plasma currents increase the iota profile. At the same time, the connection lengths in the island increase for higher plasma currents since the island moves away from the divertor. In addition, the confined region of closed field lines around the O point of the island gets increasingly large for higher plasma currents, and, in the case of $I_p = 6\,\text{kA}$, the closed field line region is entered by the probe. Correlating the topology along the probe path in figure 3 with the probe measurements in figure 2, we find that the drop of T_e from 50 eV to 25 eV in the innermost 5 mm of the profile (dark blue line) occurs exactly at the position where the probe is in the closed field line region. This observation indicates that the closed field line region in the island is a separate confinement region which accumulates particles but is not directly fuelled with energy and therefore reveals quite small T_e at relatively high densities. The highest temperature in the SOL is expected to be observed at the border between the short and long connection length region [25], which is clearly visible here in the 3 kA case: the position of the T_e peak in both data sets in figure 2(a) just short of $R = 6.08\,\text{m}$ directly corresponds to the steep increase of connection lengths on the probe path in figure 3(b) at the same radial position.

2.3. Comparison to other edge diagnostics

Having now investigated the local effects of toroidal plasma currents at the probe position, it is important to consider that these observations only represent a 1D section and are not necessarily representative for the 3D SOL of W7-X. To obtain a more global picture, other edge diagnostics are required. A selection of those is presented in figure 4 for the program 16 (blue lines in figures 1, 2), showing divertor heat fluxes from infrared (IR) thermography [27], T_e and n from divertor Langmuir probes, and parallel plasma (impurity) flow velocities from Coherence Imaging Spectroscopy (CIS). To better point out the role of the plasma current, the time traces obtained by the diagnostics have been mapped to the plasma current displayed in figure 1(c).

In figures 4(a)–(c) poloidal heat flux profiles across the strike lines are shown for three out of the ten divertors. With increasing plasma current, the strike line first (up to about 3.5 kA) moves away from the pumping gap (i.e. upwards in the figure) while the heat flux magnitude remains approximately unchanged. This behavior is typical for the W7-X island divertor and can well be explained by field line diffusion modelling [14]. At about 6kA plasma current, the heat flux patterns on the two lower divertor modules become much broader with a decreasing magnitude of overall heat flux, resembling foot-prints of a limiter-like situation where the islands are shifted towards the plasma core so that they are not intersected by the divertor anymore [14]. In the case of lower divertor module 4 in figure 4(b), this phenomenon occurs suddenly and results in a particularly broad and decreased heat flux. In the lower divertor module 1 in figure 4(a), in contrast, the change is not as sudden and strong. The disparity
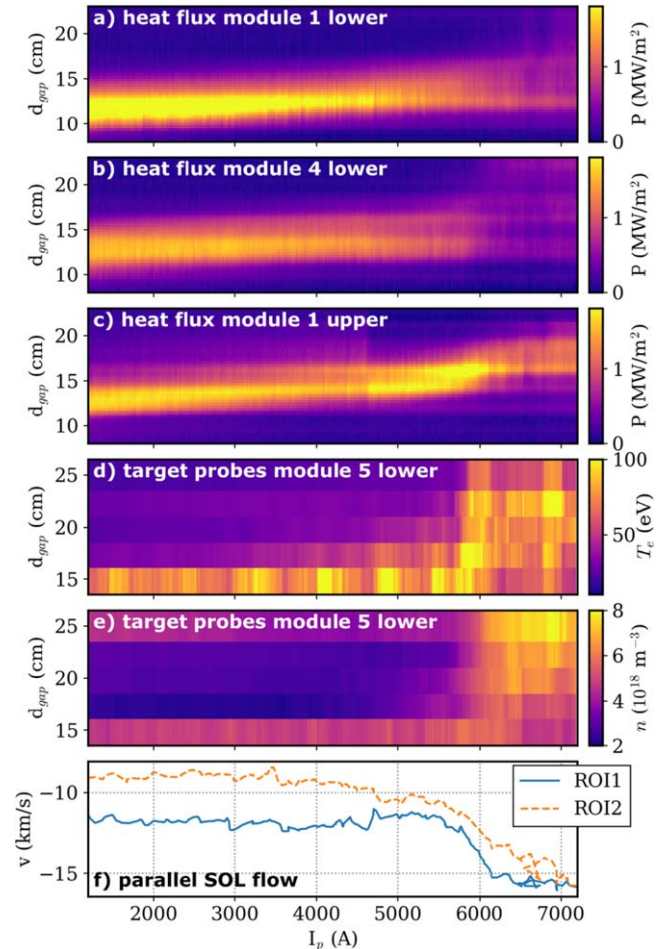

Figure 4. Divertor diagnostics results during program 20 181 010.16 as a function of toroidal plasma current: heat flux profiles across three divertor modules (a), (b), (c), electron temperature and density from divertor Langmuir probes (d), (e), plasma flow measured by CIS (f). The vertical axis in (a)–(e) denotes the distance from the pumping gap along a poloidal profile.

between these two divertor modules already hints at a toroidal asymmetry which might stem from residual error fields [28, 29]. At the upper divertor module 1 shown figure 4(c), in contrast, the heat flux pattern abruptly shifts at about 6kA plasma current. The heat flux magnitude is intermittently increased during the transition and then returns to similar values well before and well after the abrupt shift. A similar phenomenon is seen on the other four upper divertors. The striking asymmetry between upper and lower divertors can, in addition to further error field contributions, presumably be attributed to drift effects [25].

Divertor Langmuir probes are installed in the upper and lower horizontal targets of module 5 [25, 30] with two poloidal arrays of 10 probes in each location where the individual probes are separated poloidally by 25 mm. The T_e and n results from five swept probes (the ones closest to the strike line) across the lower divertor are displayed in figures 4(d), (e). In the magnetic standard configuration without toroidal plasma current, the probes do not directly cover the strike line, which is at the toroidal position of the Langmuir probes (which is different from the toroidal
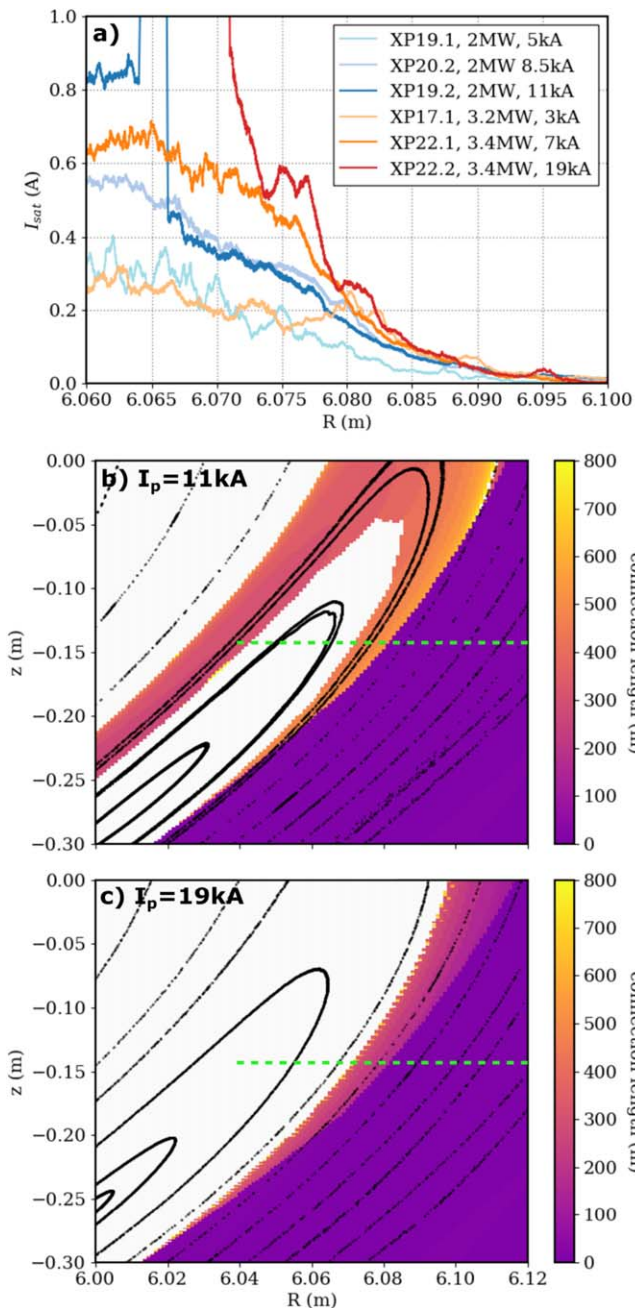
Figure 5. (a) Radial profiles of ion saturation current measured by reciprocating probe on the MPM. The red line increases up to 35 A. In the legend, the probe measurement p in the program number XP.xy on 20180816.$xy.p$ is given along with the ECR heating power and the toroidal plasma current at the time of the probe measurement. (b), (c) Poincaré plot (black dots) and connection lengths (color coded) in the R-z plane around the MPM in the W7-X standard configuration for different toroidal plasma currents, (b) 11 kA, (c) 19 kA. Light grey areas indicate closed field lines, i.e. infinite connection lengths. The probe path is indicated by the dashed green line.

position of the thermography data in (a)–(c)) situated just below the first probe. Therefore, the highest temperature and density are observed at the first probe which is closest to the strike line. However, at a plasma current of about 6 kA, the pattern of T_e and n changes suddenly towards a more even

distribution along the first five probes, indicating a shift of the plasma load on the divertor as well as a rather broad strike line. A similar observation has been made when the super-conducting planar coils of W7-X were used to increase the rotational transform starting from the standard configuration [31].

Finally, a Coherence Imaging Spectroscopy (CIS) system is able to measure the parallel flow velocity of C III impurity ions [32, 33]. The sensitivity of the (Doppler effect based) measurement is dictated by the impurity emission. As the investigated charged state photo emission coefficient peaks around $T_e \sim 10$–20 eV, CIS is sensitive to SOL flows. The carbon impurity flow is assumed to be correlated to the main plasma flow via friction forces in the density range of 10^{19} m^{-3} to 10^{20} m^{-3} [34]. While the CIS diagnostic covers a full poloidal cross section of the plasma, only two representative regions of interest (ROI) have been chosen here (see figure 7 in appendix for details). ROI2 is directly magnetically connected to the MPM with a distance of about 10m. Both data sets in figure 4(f) show an approximately constant negative flow velocity up to 5 kA plasma current, with the sign convention being defined such that negative velocities correspond to flow against the magnetic field direction. At 6 kA, the flow velocity quickly drops by about 3 km s^{-1} in both ROI. This observation agrees with the parallel Mach probe results in figure 2(e), which show an increase of the parallel Mach number profile at higher plasma current (for the probe, positive Mach numbers are defined as being against the magnetic field direction).

2.4. Summary and interpretation

Summarizing, the response of the SOL plasma to an increasing toroidal plasma current has been monitored. Even though the plasma current increases quite steadily, slowly saturating, as seen in figure 1(c), a threshold is observed around 6 kA. Above this value, a sudden change of the edge plasma parameters is seen both *upstream* with a reciprocating probe and flow measurements as well as *downstream* at the divertor target plasma parameters and heat flux distributions. The findings suggest that due to the increased iota (caused by the plasma current) the islands moved inwards (away from the divertors) such that they lost contact to the targets at some of the divertors, resulting in a sudden re-arrangement of heat and particle transport in the SOL. Although the confined plasma is not directly affected by this at first, a small increase of the line integrated density, and to a smaller degree also the diamagnetic energy, is observed, c.f. figure 1(b), when the plasma current reaches 6 kA. Upon closer inspection, also the slope of the plasma current evolution changes at this point. The density increase is presumably caused by the re-distribution of the SOL heat fluxes, which results in previously un-loaded areas of the divertor targets suddenly receiving significant heat fluxes. As a consequence, the previously untouched divertor parts heat up and start outgassing, increasing the plasma density even in the absence of external particle fuelling. We finally emphasize that these observations are well reproducible in the magnetic standard configuration and have

been observed there multiple times. The exact threshold value of the plasma current seems to vary slightly (by about 1 kA), depending on the level of the general line integrated density.

3. Driven plasma currents

Electron cyclotron current drive (ECCD) utilizes the ECRH system of W7-X to drive toroidal plasma currents non-inductively [10, 35]. This technique is advantageous for experiments on the role of plasma currents since it allows more flexible current control compared to the intrinsic bootstrap current, which evolves on rather slow time scales of some 10 s with its magnitude determined by neo-classical transport. To study the role of larger plasma currents than in the previous section, co-ECCD close to the plasma center has been employed. Here, co-ECCD is defined similarly to tokamaks, such that it points in the same direction as the bootstrap current.

Again, a sequence of experiments with similar heating power and density has been performed where the MPM measured at different time instances during the evolution of the toroidal current. The ratio of driven and bootstrap current is in all cases $\geqslant 2$, allowing the investigation of toroidal plasma currents up to 19 kA. The SOL plasmas were probed with a retarding field analyzer (RFA) probe [36] which in addition to the RFA unit contained three Langmuir probe pins on the front plate of the probe head. In figure 5(a), the radial profiles of ion saturation current along the probe path are shown for two sets of experiments with similar line integrated densities around $n_{dl} = 2.5 \cdot 10^{19} \text{m}^{-2}$. At each heating power level, three fast plunges at different plasma currents have been performed. Comparing the probe results, the ion saturation current measured by the probe is found to increase for higher plasma currents at certain set of heating and density. The probe currents at the highest plasma currents reach up far above the displayed scale and go up to $I_{i,sat} = 5$ A for $I_p = 11$ kA and $I_{i,sat} = 35$ A for $I_p = 19$ kA.

The 2D connection length map and Poincaré plots in the vicinity of the probe for these two plasma currents are shown in figures 5(b) and (c), similar to figure 3. At $I_p = 11$ kA, the magnetic island has moved so far inwards that large parts of the island are not touching the divertor anymore. At $I_p = 19$ kA, the island entirely loses contact with the divertor and is now inside the LCFS, i.e. closed flux surfaces appear outside the island, and the plasma boundary is now limited by the divertor. The probe plunge path indicated in figure 5(c) extends about 3 cm into the confined plasma, which explains the extraordinarily high ion saturation currents measured by the probe.

For completeness, we note that in the measurement at $I_p = 19$ kA the line integrated density had almost doubled compared to all the other measurements, likely due to outgassing of components which received significant heat loads for the first time due to current-induced changes of the heat load distribution patterns [14]. However, this difference in line integrated density does not play an import role for our observations of strongly qualitatively different profiles.
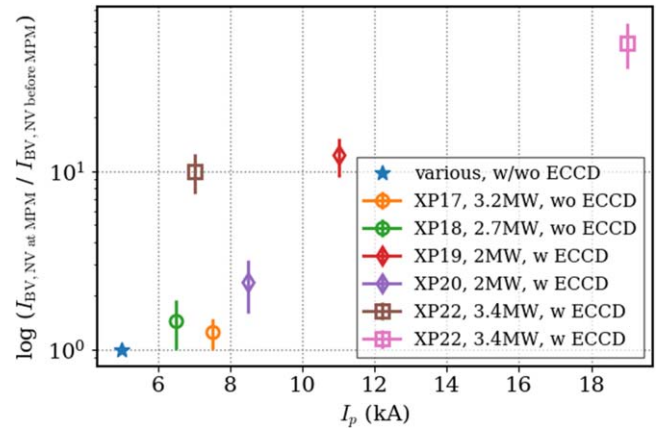

Figure 6. Increase of boron and nitrogen line intensities measured by HEXOS due to MPM probe plunge as a function of plasma current. All probe plunges had a similar depth. In the legend, the program number XP.*xy* on 20180816.*xy* is given along with the ECR heating power and whether ECCD was applied.

A further indicator for the strength of the probe-plasma interaction is the release of impurities due to excess heat flux on the probe. Since the probe head body was made of boron nitride, boron and nitrogen are the dominating impurity species released from the probe. The VUV spectrometer HEXOS is able to detect changes in the level of nitrogen and boron impurities with a high sensitivity and a good temporal resolution of 1 ms [37]. In figure 6, the relative increase of the B V and N V line intensities due to the probe plunge as measured by HEXOS are shown on a logarithmic scale for various probe plunges at different toroidal plasma currents. All probe plunges had the same depth and were conducted at similar line integrated plasma densities. The respective heating power levels and whether the plasma current stems from ECCD or bootstrap current evolution is given in the legend. A general trend towards an increasing impurity line radiation for probe plunges at higher plasma currents is observed. In a simple approximation, the impurity line intensities can be taken as a measure for the impurity concentration, since only situations where the plasma temperature and density have not been strongly changed by the probe operation have been used for the data points shown here. Concluding, for similar probe plunges at similar plasma conditions, both the ion saturation currents measured by the probe and impurity release from the probe head body is observed for higher plasma currents. A detailed investigation of SOL parameters as in section 2 is unfortunately not possible for the programs with higher (driven) toroidal currents due to insufficient diagnostic coverage and remains to be studied in the upcoming operation phases of W7-X.

4. Summary and conclusion

The role of toroidal plasma currents for the W7-X SOL is investigated for the magnetic standard configuration using reciprocating and target Langmuir probes, divertor thermography, and plasma flow measurements in experiments where

plasma density and heating remained constant. Field line tracing predicts that toroidal plasma currents increase the rotational transform profile and therefore affect the position of the edge islands and the connection length distribution in the island divertor. At the position of the reciprocating probe close to the outer mid-plane, increasing plasma currents result in both higher T_e and n. At a plasma current of about $6 \pm 1 \, kA$, the confining region of closed field lines inside the edge island has become sufficiently large to be crossed by the reciprocating probe, revealing a dense, but cooler plasma inside this region and a modification of the poloidal plasma dynamics in the open field line region of the island. At the same plasma current level, other edge diagnostics observe a sudden change of divertor heat loads and plasma flows, qualitatively consistent with the probe observations. Higher plasma currents up to 19 kA have been obtained employing ECCD. At these conditions, the edge islands are predicted to move into the LCFS of the main plasma, resulting in a transition from a diverted to a limited plasma configuration. This hypothesis is plausibly supported by reciprocating probe measurements.

These observations highlight the importance of toroidal plasma currents and emphasize the requirement of a fine control of the rotational transform for island divertor operation.

Acknowledgments

Appendix

The coherence imaging spectroscope (CIS) is a 2D interferometer. By using birefringent plates, a fringe pattern is overlaid on a camera view of the plasma. The CIS is able to monitor the behaviour of ions, by selecting single charged state of single species with a narrowband filter. The W7-X CIS system used for the presented studies is characterized by a toroidal view, allowing flow velocity measurements dominated by the parallel component [32, 33]. It provides line of sight integrated flow velocities in the SOL which are inferred from the Doppler shift of CIII impurity emission. Two measurement results are presented in figure 7, which have been taken at the time instances of the probe plunges in program 16 of figures 2, 4. Each plot resembles a full cross-sectional view in the region of the lower divertor in module 3 (covering approximately one full module of W7-X along the optical axis), revealing a pattern of co- and counter-streaming regions which are characteristic for the island divertor [33]. Comparing both plots, one finds that at the later time instance (at higher plasma current), the parallel flow pattern generally gets
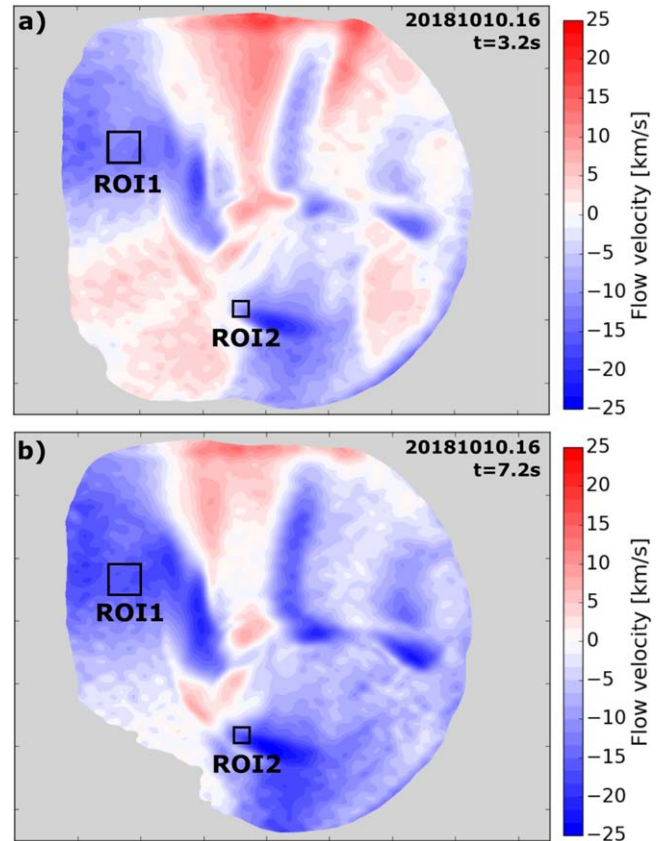

Figure 7. Parallel plasma flow patterns measured by coherence imaging spectroscopy at the time instants of the probe plunges in the same plasma program (20 181 010.16) as in figures 2, 4. Positive plasma flows are defined as along the magnetic field, i.e. into the image plane. From the regions of interest marked here the traces in 4(f) were taken. ROI2 corresponds to the position of the MPM probe mapped along the magnetic field.

more negative, i.e. tends to flow against the magnetic field, out of the image plane. This is consistent with the Mach probe measurements presented in figure 2.

The agreement is further corroborated by the CIS traces shown in figure 4 which are taken from the region of interest (ROI) marked in figure 7. In particular, ROI2 is selecting the lines of sight that are intersecting the same magnetic island crossed by the reciprocating probe (which is located about 10 m away along the field lines). A more detailed investigation on the mapping between CIS and reciprocating probes is presented in [32]. Flow velocity evolution in this ROI is generally expected to match the effect measured by the probe, assuming that the distance between both diagnostics is much smaller than the distance to the stagnation point. More quantitative investigations into cross validation of CIS and Mach probes require to disentangle the exact 3D mapping (possibly incorporating magnetic error fields), the role of the line-integrating nature of the CIS and the possible discrepancy between flows of impurities (as measured by CIS) and the main plasma species (as measured by Mach probes), which is outside the scope of this paper and will be addressed in a future publication.

ORCID iDs

Carsten Killer ⬤ https://orcid.org/0000-0001-7747-3066
Yu Gao ⬤ https://orcid.org/0000-0001-8576-0970
Valeria Perseo ⬤ https://orcid.org/0000-0001-8473-9002
Lukas Rudischhauser ⬤ https://orcid.org/0000-0002-3696-7067
Kenneth Hammond ⬤ https://orcid.org/0000-0002-1104-4434
Birger Buttenschön ⬤ https://orcid.org/0000-0002-9830-9641
Philipp Drews ⬤ https://orcid.org/0000-0002-6567-1601
Michael Endler ⬤ https://orcid.org/0000-0003-2314-8393
Joachim Geiger ⬤ https://orcid.org/0000-0003-4268-7480
Marcin Jakubowski ⬤ https://orcid.org/0000-0002-6557-3497
Jens Knauer ⬤ https://orcid.org/0000-0001-7359-6472
Holger Niemann ⬤ https://orcid.org/0000-0003-0300-1060
Matthias Otte ⬤ https://orcid.org/0000-0003-3134-7579
Kian Rahbarnia ⬤ https://orcid.org/0000-0002-5550-1801

References

[1] König R *et al* 2002 *Plasma Phys. Control. Fusion* **44** 2365
[2] Grieger G *et al* 1992 *Physics of Fluids B: Plasma Physics* **4** 2081–91
[3] Geiger J, Beidler C D, Feng Y, Maaberg H, Marushchenko N B and Turkin Y 2015 *Plasma Phys. Control. Fusion* **57** 014004
[4] Geiger J, Beidler C, Drevlak M, Maaßberg H, Nührenberg C, Suzuki Y and Turkin Y 2010 *Contrib. Plasma Phys.* **50** 770–4
[5] Geiger J *et al* 2012 *Plasma Phys. Control. Fusion* **55** 014006
[6] Turkin Y, Maassberg H, Beidler C D, Geiger J and Marushchenko N B 2006 *Fusion Sci. Technol.* **50** 387–94
[7] Dinklage A *et al* 2018 *Nat. Phys.* **14** 855–60
[8] Klinger T *et al* 2019 *Nucl. Fusion* **59** 112004
[9] Erckmann V, Gasparino U and MaaBberg H 1992 *Plasma Phys. Control. Fusion* **34** 1917–23
[10] Wolf R C *et al* 2018 *Plasma Phys. Control. Fusion* **61** 014037
[11] Sinha P, Böckenhoff D, Endler M, Geiger J, Hölbe H, MSmith H, SPedersen T and Turkin Y 2019 *Nucl. Fusion* **59** 126012
[12] Lore J D *et al* 2014 *IEEE Trans. Plasma Sci.* **42** 539–44
[13] Hölbe H, Pedersen T S, Geiger J, Bozhenkov S, König R, Feng Y, Lore J and Lumsdaine A 2016 *Nucl. Fusion* **56** 026015
[14] Gao Y *et al* 2019 *Nucl. Fusion* **59** 106015
[15] Renner H, Sharma D, Kilinger J, Boscary J, Grote H and Schneider R 2004 *Fusion Sci. Technol.* **46** 318–26
[16] Pedersen T S *et al* 2019 *Nucl. Fusion* **59** 096014
[17] Nicolai D *et al* 2017 *Fusion Eng. Des.* **123** 960–4 proceedings of the 29th Symposium on Fusion Technology (SOFT-29) Prague, Czech Republic, September 5–9, 2016
[18] Killer C, Grulke O, Drews P, Gao Y, Jakubowski M, Knieps A, Nicolai D, Niemann H, Sitjes A P and Satheeswaran G 2019 *Nucl. Fusion* **59** 086013
[19] Drews P *et al* 2019 *Nuclear Materials and Energy* **19** 179–83
[20] Stroth U 1998 *Plasma Phys. Control. Fusion* **40** 9–74
[21] Hirsch M *et al* 2008 *Plasma Phys. Control. Fusion* **50** 053001
[22] Narushima Y *et al* 2011 *Nucl. Fusion* **51** 083030
[23] Endler M *et al* 2015 *Fusion Eng. Des.* **100** 468–94
[24] Barbui T *et al* 2019 *J. Instrumen.* **14** C07014
[25] Hammond K C *et al* 2019 *Plasma Phys. Control. Fusion* **61** 125001
[26] Effenberg F *et al* 2017 *Nucl. Fusion* **57** 036021
[27] Gao Y, Jakubowski M, Drewelow P, Pisano F, Sitjes A P, Niemann H, Ali A and Cannas B 2019 *Nucl. Fusion* **59** 106015
[28] Lazerson S A *et al* 2017 *Nucl. Fusion* **57** 046026
[29] Bozhenkov S, Lazerson S, Otte M, Gates D, Pedersen T S and Wolf R 2016 *Nucl. Fusion* **56** 076002
[30] Laube R, Laux M, Ye M Y, Greuner H and Lindig S 2011 *Fusion Eng. Des.* **86** 1133–6 proceedings of the 26th Symposium of Fusion Technology (SOFT-26)
[31] Lazerson S A *et al* 2019 *Nucl. Fusion* **59** 126004
[32] Perseo V, Gradic D, König R, Ford O P, Killer C, Grulke O and Ennis D A 2019 *Rev. Sci. Instr.* submitted to
[33] Perseo V, Effenberg F, Gradic D, König R, Ford O P, Reimold F, Ennis D, Schmitz O and Pedersen T S 2019 *Nucl. Fusion* **59** 124003
[34] Feng Y *et al* 2006 *Nucl. Fusion* **46** 807–19
[35] Zanini M *et al* 2019 *EPJ Web Conf.* **203** 02013
[36] Henkel M, Höschen D, Liang Y, Li Y, Liu S, Nicolai D, Sandri N, Satheeswaran G, Yan N and Zhang H X 2018 *Plasma Sci. Technol.* **20** 054001
[37] Biel W, Bertschinger G, Burhenn R, König R and Jourdain E 2004 *Rev. Sci. Instrum.* **75** 3268–75